J. Cent. South Univ. (2020) 27: 3118−3132
DOI: https://doi.org/10.1007/s11771-020-4533-5

Springer

Effect of loading rate on fracture behaviors of shale under mode I loading

XIE Qin(谢秦)[1], LI Sheng-xiang(李生相)[1], LIU Xi-ling(刘希灵)[1],
GONG Feng-qiang(宫凤强)[2], LI Xi-bing(李夕兵)[1]

1. School of Resources and Safety Engineering, Central South University, Changsha 410083, China;
2. School of Civil Engineering, Southeast University, Nanjing 211189, China

Abstract: In this study, the effect of loading rate on shale fracture behaviors was investigated under dynamic and static loading conditions. Cracked straight through Brazilian disc (CSTBD) shale specimens were tested with a split Hopkinson pressure bar (SHPB) setup and INSTRON1346 servo-testing machine under pure mode I loading conditions. During the test, the crack propagation process was recorded by high-speed (HS) camera, and the acoustic emission (AE) signal generated by the fracture was collected by acoustic emission (AE) system. At the same time, crack propagation gauge (CPG) was used to measure the crack propagation velocity of the specimen. The results show that the crack propagation velocity and fracture toughness of shale have a positive correlation with the loading rate. The relationship among the crack propagation velocity, the fracture toughness and the loading rate is established under the static loading condition. In addition, the characteristics of AE signals with different loading rates are analyzed. It is found that the AE signals generated by microcrack growth decrease with the increase of loading rates. Meanwhile, the turning point of cumulative counting moves forward as the loading rate increases, which shows that the AE signal generated by shale fracture at low loading rate mainly comes from the initiation and propagation of microcracks, while at high loading rate it mainly comes from the formation of macro large-scale cracks. The fracture mechanism that causes shale fracture toughness and crack propagation velocity to vary with loading rate is also discussed based on the analysis results of AE signals.

Key words: shale; loading rate; cracked straight through Brazilian disc; fracture toughness; acoustic emission; crack propagation velocity

Cite this article as: XIE Qin, LI Sheng-xiang, LIU Xi-ling, GONG Feng-qiang, LI Xi-bing. Effect of loading rate on fracture behaviors of shale under mode I loading [J]. Journal of Central South University, 2020, 27(10): 3118−3132. DOI: https://doi.org/10.1007/s11771-020-4533-5.

1 Introduction

It is well known that the loading rate is one of the most important factors affecting the mechanical properties of rock materials. A large number of research results have shown that it will enhance the strength of rock as the loading rate increases [1−5]. However, there are many micro-defects or fissures inside in the process of geological evolution of natural rocks. The process of rock fracture and instability is completed by internal micro-cracks under a certain loading condition through initiation, crack propagation, connection and formation of a macroscopic penetrating fracture surface [6, 7]. Therefore, considering the loading rate effect of rock with the knowledge of fracture mechanics can be more helpful to understand the internal mechanism of the change of rock mechanical properties.

In the field of fracture mechanics, fracture toughness is a mechanical property index to

Foundation item: Project(41630642) supported by the National Natural Science Foundation of China
Received date: 2020-06-12; **Accepted date:** 2020-09-13
Corresponding author: LIU Xi-ling, PhD, Associate Professor; Tel: +86-731-88879612; E-mail: lxlenglish@163.com; ORCID: https://orcid.org/0000-0002-0159-8177

measure the ability of material to resist crack instability. In the laboratory, the fracture toughness is determined by the stress intensity factor when the crack begins to propagate. Because mode I fractures are the most common fracture mode, many scholars have done a lot of relevant research work on loading rate effect on rock mode I fracture toughness, which also obtained the important theoretical results [8−13]. ZHANG et al [9] conducted a dynamic fracture test on marble with a modified split Hopkinson pressure bar (SHPB) setup, which showed that the rock fracture toughness increased linearly with increasing loading rate. YIN et al [11] considered the dynamic fracture behaviour of granite with different loading rates under a given preload, in which cracked straight-through Brazilian disc (CSTBD) specimens were selected for dynamic fracture test that was carried out on a dynamic and static coupling test device based on the SHPB system. The experimental results are consistent with those of ZHANG et al [9]. ZHOU et al [12] investigated the effect of rock moisture content and loading rate on rock fracture toughness. Dynamic fracture tests of notched semi-circular bending (NSCB) sandstone specimens under different impact velocities were carried out with the modified SHPB setup. It was found that the fracture toughness and dynamic propagation toughness of sandstone increased as the loading rate increased. Although the experimental methods and the materials studied above are quite different, it can be agreed that the fracture toughness of the materials increases with the increase of the loading rate. Meanwhile, in the dynamic loading test, because the distribution of the stress field at the crack tip is affected by the crack propagation velocity, in order to achieve the dynamic propagation toughness of rock specimens, it is necessary to determine the crack propagation velocity at a certain moment [14]. In this process, many scholars found that there was a certain relationship between crack propagation velocity and loading rate. ZHOU et al [12] determined the crack propagation velocity of sandstone with the digital image correlation (DIC) technique under dynamic loading conditions, and found that there was a linear positive correlation between the crack propagation velocity and the loading rate. JU et al [15] measured the crack propagation velocity of rock with crack propagation gauge (CPG) technology under different impact pressure by using SHPB setup, and concluded that the crack propagation velocity has a positive correlation with the impact pressure. The conclusions mentioned above are all obtained under dynamic loading conditions, but few studies discuss the effect of loading rate on crack propagation velocity and fracture toughness under static loading conditions. In fact, most of the rock mechanical tests are carried out at low loading rate. It is helpful to understand the changing process of rock mechanical properties to conduct static fracture tests at different loading rates. Therefore, it is necessary to study the effect of loading rate on rock fracture behavior under static and dynamic loading.

The effect of loading rate on shale fracture behaviors under dynamic and static loading conditions was discussed in this study. Dynamic fracture testing was conducted on a modified SHPB setup, while static fracture testing was conducted on INSTRON1346 servo-testing machine. Fracture toughness was determined by using cracked straight through Brazilian disc (CSTBD) method. The failure process and acoustic emission (AE) signals of shale specimens under different loading rates were recorded, and crack propagation gauge (CPG) was used to determine the crack propagation velocity. In addition, according to the test results, the relationship among fracture toughness, crack propagation velocity, AE characteristics and loading rate were analyzed and discussed.

2 Experimental program

2.1 Testing method and specimen preparation

Four standard test procedures and methods for testing the mode I static fracture toughness of rock materials have recommended by the International Society for Rock Mechanics (ISRM), namely cracked chevron notched Brazilian disc (CCNBD) method, chevron bend (CB), notched semi-circular bending (NSCB) method and short rod (SR) methods, respectively [16−18]. In fact, due to the different loading methods and loading devices, the method of measuring fracture toughness under static conditions is difficult to be extended to dynamic loading conditions. In order to facilitate the testing of fracture toughness under dynamic

loading conditions, many scholars have proposed a lot of methods for determining dynamic fracture toughness, such as CCNBD method [17], semi-circular bend (SCB) method [19], cracked chevron notched semi-circular bending (CCNSCB) method [20] and cracked straight-through Brazilian disc (CSTBD) method [10, 21, 22]. Due to its simple configuration, easy fabrication and processing, and the existence of analytical solutions to the calculation of stress intensity factor, the CSTBD method has been widely used in the testing of fracture toughness in dynamic impact test. In view of the above advantages, the CSTBD method was selected to determine the fracture toughness of shale under different loading rates in this study.

All CSTBD specimens were taken from the same shale rock mass, which has high geometric integrity and uniformity. First, a core with a standard diameter of 60 mm was drilled, and then it was cut into a disc with an average thickness of 30 mm. A slot with a length of 10 mm was cut symmetrically from the center of the original disc. Finally, the tip of the incision was further sharpened with a diamond wire to form a crack tip. The schematic diagram of the CSTBD specimen is shown in Figure 1.

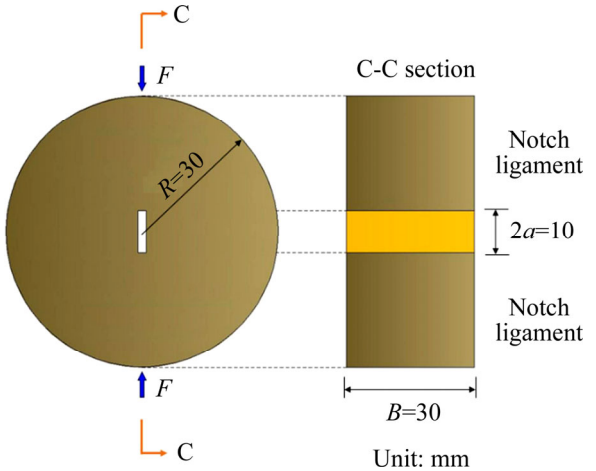

Figure 1 Schematic of CSTBD specimen (notch width is less than 1.5 mm)

2.2 Loading apparatus and crack propagation measurement techniques

In order to investigate the change of fracture behaviors of shale specimens from low loading rate to high loading rate, rock mechanics tests under dynamic and static loading conditions were carried out in this study. The static test was conducted on INSTRON1346 servo-testing machine, and the dynamic test was conducted on a modified SHPB setup [23−25]. According to the loading limit of the testing machine, five loading rates were set in the static test, the minimum was 30 N/s, and the maximum was 30 kN/s, while the dynamic fracture test was only carried out under one impact pressure. In order to ensure that the rock specimen is broken into two parts after failure, 0.28 MPa was selected as the impact pressure after repeated tests. The specific loading rate under static and dynamic loading conditions is shown in Table 1.

Table 1 Loading rate under static and dynamic loading conditions

Load type	Loading rate/(N·s^{-1})	Impact pressure/MPa
Static load	30	–
	165	–
	300	–
	3000	–
	30000	–
Dynamic load	–	0.28

The schematic diagram of the experimental devices for static and dynamic testing are shown in Figure 2. It can be found that the experimental devices contain a crack propagation velocity measurement system, a digital image correlation (DIC) system and an AE system. The following section introduces the details of the main test technology and devices.

2.2.1 High-speed digital image correlation technique

Digital image correlation (DIC) technology was mainly proposed by RANSON in 1960s [26], and is now mostly used in mechanical properties experiments of metals, composite materials and rocks [27−29]. Based on the image before and after the deformation of the object, the spatial position of the point before and after the deformation is determined according to the probability and statistical correlation of the randomly distributed speckle on the surface, so as to calculate the displacement and strain of the point, and obtain the displacement field and strain field of the object surface. Compared with the traditional scanning electron microscope (SEM) and CT imaging

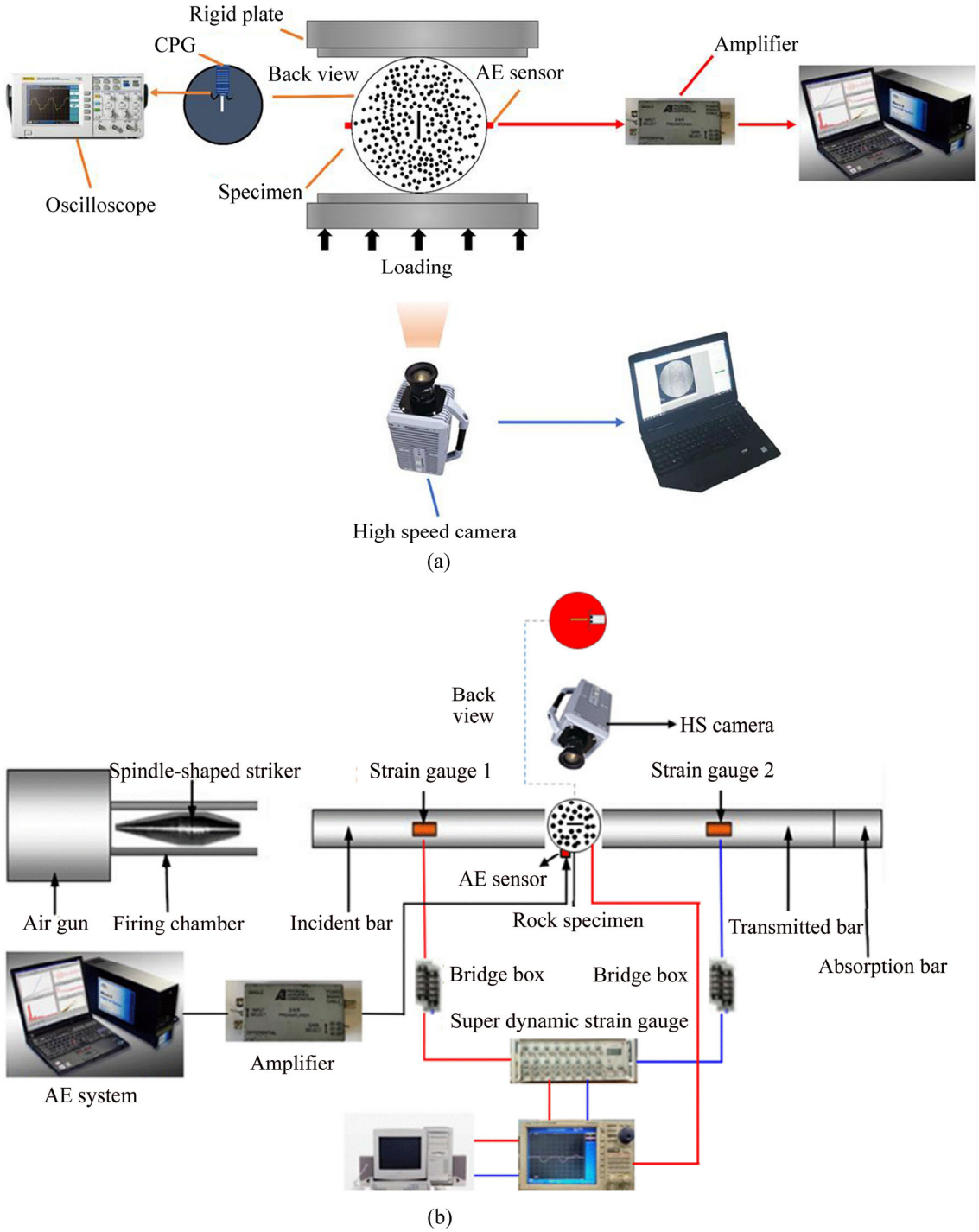

Figure 2 Experimental setup for the fracture test: (a) Static loading; (b) Dynamic loading modified from Refs. [24, 25]

methods, the digital speckle method can realize the non-contact, high precision and automatic measurement, at the same time, has low requirements for the measurement environment, strong anti-interference ability. In view of the above advantages, this study used DIC technology to analyze the strain field of shale specimens.

Due to the limited sampling time of the HS camera, in order to record the entire destruction process of the rock under static loading conditions, the HS camera must be manually triggered to record the picture before the rock is about to fail. The HS camera captured images at a frequency of 79161 frames/s with a resolution of 256 pixel× 256 pixel under static loading condition, while under dynamic loading condition, the HS camera captured images at a frequency of 100000 frames/s with a resolution of 128 pixel×256 pixel. The ratio

of real length to the image size is equal to 0.28 mm/pixel. The images captured by HS camera were processed with the open source 2D-DIC MATLAB software (Ncorr v1.2). In addition, in order to ensure that the image has obvious contrast, in the specimen preparation process, first, a very thin white bottom layer was sprayed on the front surface of the specimen, and then a black marker was used to randomly create speckles on the white bottom layer.

2.2.2 Crack propagation velocity measurement system

The crack propagation gauge (CPG) has many advantages in testing the crack propagation velocity and crack initiation time. It has high sensitivity, accurate monitoring range, simple operation and only occupies one oscilloscope data acquisition channel. Many scholars used this test technology to measure crack propagation velocity [15, 30−32].

In this test, CPG technology was used to determine the crack propagation velocity, with working principle shown in Figure 3. The initial resistance of CPG is about 5 Ω, which is composed of 15 metal grid wires with different width but the same length in parallel. The distance between two adjacent grid wires is ΔL=1.5 mm. In order to accurately measure the crack propagation velocity of the material, the predicted crack propagation area was first polished with sandpaper, and CPG was closely adhered to the surface of the material. Finally, CPG was connected to a circulating circuit that can provide 16 V constant voltage. In the circulating circuit, the resistance of R_1 and R_2 is 50 Ω to ensure that the CPG power will not burn out the circuit.

When the crack propagates to the sticking area of CPG, the first wire of CPG will be pulled off, which will change the resistance of CPG, further change the voltage signal, and generate step voltage signal. The voltage of CPG increases gradually as the crack propagates forward. The voltage signal is recorded by an oscilloscope with the sampling frequency of 10 MHz.

2.2.3 Acoustic emission system

After the rock is subjected to internal or external load or deformation, it forms energy accumulation [33]. When it reaches a certain level, part of the strain energy will be released outwards in the form of elastic waves, which is called acoustic emission (AE) activity. The recorded acoustic emission signal waveform carries information about rock damage, and many characteristic parameters of AE signals can better describe the failure process of materials and reflect their real-time morphology during the failure process [34−38]. Importantly, the change of loading rate will lead to the change of rock fracture mechanism. Therefore, the AE signals generated by rock fracture are also different under various loading rates.

In this experiment, the acoustic emission system mainly consists of two AE sensors, two preamplifiers and an AE signal acquisition

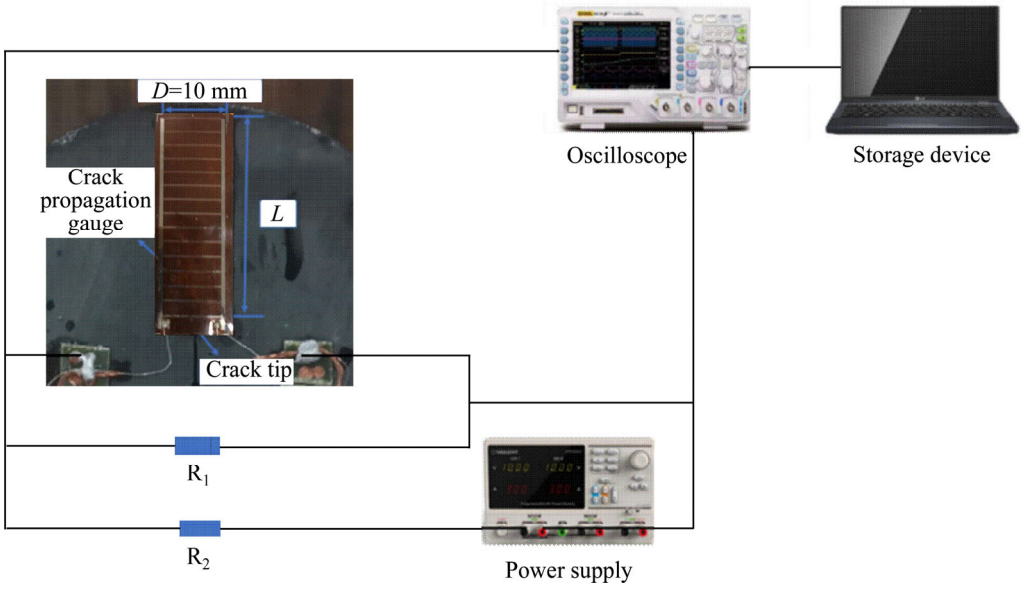

Figure 3 Crack propagation velocity measurement system

equipment. The AE sensor was tightly attached to the surface of the rock specimen to accurately record the AE signals generated by the fracture of the specimen during the loading process. In addition, in order to reduce the influence of noise generated by the external environment on the experimental results, the threshold set by the acoustic emission device in the static fracture test is 40 dB, that is, when the amplitude of AE signal exceeds 40 dB, it can be regarded as a valid AE event. However, the threshold value of the acoustic emission system for the dynamic fracture test is set to 45 dB, because it is easier to generate high amplitude noise signals. The specific parameter settings of acoustic emission equipment are shown in Table 2.

Table 2 Parameter settings of acoustic emission device

Threshold/dB	Pre-gain/dB	Sample length/kb	Sample frequency/MHz
40, 45	40	5	10
PDT/μs	HLT/μs	HDT/μs	
50	300	200	

3 Result and discussion

3.1 Mechanical behavior of shale with different loading rates

In fact, only the experimental results of shale specimens that begin to crack from the crack tip are effective. In this test, because of the high sampling frequency of high-speed (HS) camera, the image resolution is too low, so it is difficult to judge whether specimens crack from the crack tip directly with the naked eye, or to analyze the whole failure process of specimens. In order to solve this problem, DIC technology was used to analyze the strain field of shale specimens.

The evolution of horizontal strain field of shale specimen with loading rate of 300 N/s over time is shown in Figure 4. Because the HS camera cannot be synchronized with the loading apparatus under the static loading condition, this study used the time point of the first photo taken after the high-speed camera is triggered for subsequent analysis. It can be found that the strain at the crack tip is larger than that in other regions at 0 μs, indicating that the stress concentration at the crack tip is relatively obvious, while with the increase of the load, the local strain begins to spread towards the loading point, and reaches the loading point at 425 μs. In this process, the horizontal strain at the crack tip is always the largest, which indicates that the failure of shale specimen first occurs at the crack tip and then extends to the whole specimen.

From the DIC analysis results of all shale specimens, it is found that the local strain spreading processes of shale specimens under different loading rates are very similar, and the small

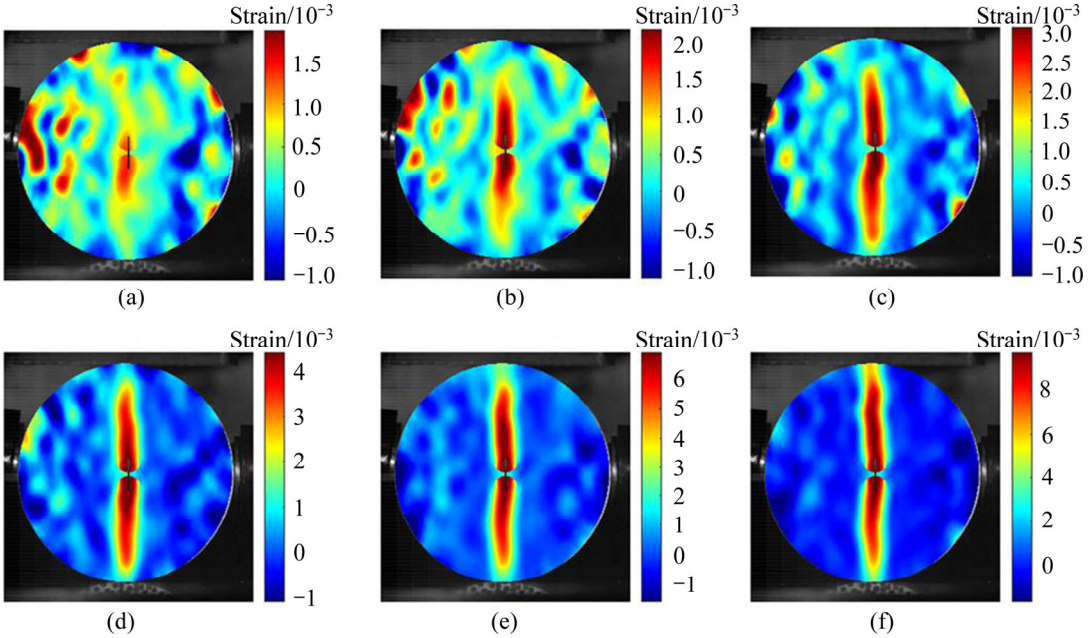

Figure 4 Evolution process of horizontal strain field of S-3-1 shale specimen: (a) 0; (b) 362.5 μs; (c) 387.5μs; (d) 400 μs; (e) 412.5 μs; (f) 425 μs

difference lies in the different spreading paths and the length of spreading time. Therefore, the evolution processes of horizontal strain field of shale specimens under other loading rates are not analyzed and discussed here.

Figure 5 shows the load−displacement curve of shale under different loading rates. It can be clearly seen that under the static loading condition, the load−displacement curves of shale specimens change from concave to convex before the peak load, and drop sharply after the peak load. This shows that the state of shale specimen changes from ductility to elasticity under static loading condition, but it is opposite under dynamic impact loading. This indicates that shale specimens show more brittleness at low loading rate, but gradually transform into ductility at high loading rate.

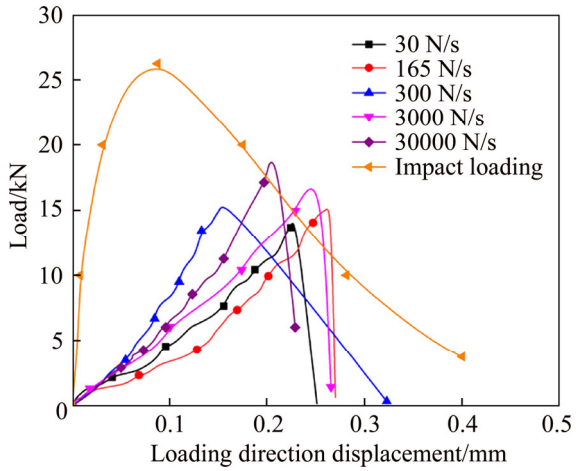

Figure 5 Load−displacement curves of shale with different loading rate

3.2 Fracture toughness of shale with different loading rates

The stress intensity factor (SIF) can well describe the stress field at the crack tip. With the increase of load F, the SIF increases. When the SIF is equal to the fracture toughness of the material, the crack begins to propagate. Fracture toughness is usually calculated based on the peak load F_{max} of the specimen. The fracture toughness K_{IC} of CSTBD specimens can be calculated according to the following formula [39]:

$$K_{IC}=Y\left(\frac{a}{R}\right)\frac{F_{max}\sqrt{\pi a}}{\pi BR} \tag{1}$$

$$Y\left(\frac{a}{R}\right)=\left[1-0.5\frac{a}{R}+1.56\left(\frac{a}{R}\right)^2-3.18\left(\frac{a}{R}\right)^3+10.1\left(\frac{a}{R}\right)^4-20.78\left(\frac{a}{R}\right)^5+20.13\left(\frac{a}{R}\right)^6-7.51\left(\frac{a}{R}\right)^7\right]\Big/\sqrt{1-\frac{a}{R}} \tag{2}$$

where R is the radius of CSTBD specimen, B is the thickness of specimen, and a is half of the initial crack length of specimen.

By processing the original data, the experimental results of shale specimens under different loading rates are obtained, as shown in Table 3. It can be found that the fracture toughness of shale has a positive correlation with loading rate. The fracture toughness of the specimen is 0.74 MPa·m$^{1/2}$ when the loading rate is 30 N/s. when the loading rate reaches 30000 N/s, the fracture toughness of the specimen rises to 0.93 MPa·m$^{1/2}$, which is 125.6% of the loading rate of 30 N/s, while the fracture toughness of the specimen under dynamic loading is 1.26 MPa·m$^{1/2}$, which is 170% of the loading rate of 30 N/s. The above test results show that the fracture toughness of the specimens under static loading is much smaller than that under dynamic loading, even under static loading conditions, the influence of

Table 3 Test results of shale specimens in fracture test

Loading rate/(N·s^{-1})	Specimen No.	K_{IC}/(MPa·m$^{1/2}$)		V/(m·s^{-1})	
		Test	Ave.	Test	Ave.
30	S-1-1	0.686	0.732	201.5	226.6
	S-1-2	0.783		240.5	
	S-1-3	0.729		237.9	
165	S-2-1	0.838	0.773	311.5	301.6
	S-2-2	0.707		292.1	
	S-2-3	0.772		301.4	
300	S-3-1	0.736	0.799	318.4	332.5
	S-3-2	0.816		325.8	
	S-3-3	0.845		353.4	
3000	S-4-1	0.803	0.845	410.7	423.1
	S-4-2	0.861		428.1	
	S-4-3	0.871		430.5	
30000	S-5-1	0.883	0.926	520.2	530.6
	S-5-2	0.953		540.5	
	S-5-3	0.943		531.2	
Impact loading	S-6-1	1.212	1.26	724.1	744.7
	S-6-2	1.305		762.7	
	S-6-3	1.265		747.3	

loading rate on fracture toughness is significant.

In order to accurately predict the fracture toughness of shale specimens under different loading rates, the exact relationship between the two should be expressed by a mathematical formula. Since the loading rate under dynamic loading is several orders of magnitude different from that under static loading, only the mathematical relationship between the loading rate and shale fracture toughness under static loading is established. In addition, because the loading rate span of static test is too large, the maximum loading rate is 1000 times the minimum loading rate, so it is difficult to see the functional relationship between the loading rate and the fracture toughness of the specimen through the graph drawn by the original loading rate data. In this study, the original loading rate is transformed according to Eq. (3), and then the subsequent analysis is carried out:

$$T_{\mathrm{LR}}=\lg\frac{L_{\mathrm{R}}}{3} \tag{3}$$

where T_{LR} is the transformed loading rate and L_{R} is the original loading rate.

The change rule of fracture toughness of shale specimen with the transformed loading rate under static loading condition is shown in Figure 6. It is easy to see that the two have obvious linear relationship. After calculation, the correlation coefficient of the fitting equation based on the linear regression model is 0.989, which shows that the relationship between the average fracture toughness and the transformed loading rate can be expressed as a linear function:

$$K_{\mathrm{IC}}=0.66634+0.06334T_{\mathrm{LR}} \tag{4}$$

Substituting Eq. (3) into Eq. (4), the relationship between the original loading rate and the fracture toughness is as follows:

$$K_{\mathrm{IC}}=0.636634+0.06334\lg L_{\mathrm{R}} \tag{5}$$

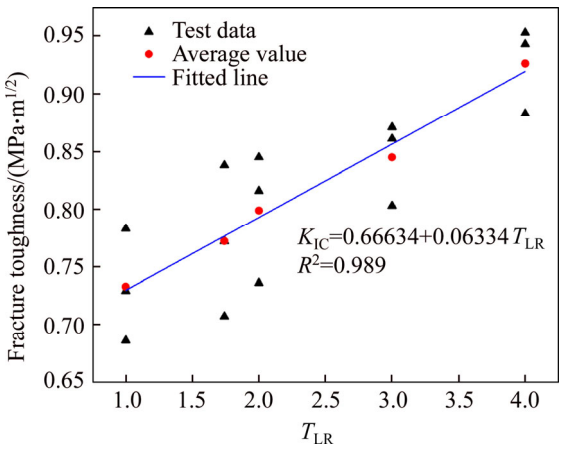

Figure 6 Variation of fracture toughness versus loading rate under static loading

Under dynamic loading conditions, according to the method of determining the loading rate recommended by ISRM [19], the loading rate of the shale specimen in this test at an impact pressure of 0.28 MPa is about 0.57 GN/s. Through the mathematical relationship between the fracture toughness and loading rate derived under static loading conditions, the predicted value of the fracture toughness of the shale specimen under dynamic loading conditions is 1.19 MPa·m$^{1/2}$, while the test value in this test is 1.26 MPa·m$^{1/2}$. The difference between the two is only 0.07 MPa·m$^{1/2}$. It shows that the mathematical relationship between the fracture toughness of shale and loading rate may be the same under dynamic loading and static loading conditions, and more experimental data from dynamic tests are needed to verify.

The final failure pictures of shale specimens at different loading rates are shown in Figure 7. It can be found that when the loading rate is low, the crack does not propagate forward in a straight line along the surface of the prefabricated crack after it starts from the tip of the prefabricated crack, and the crack propagation path is relatively zigzag. However, with the increase of the loading rate, the crack propagation path becomes straight. This result is consistent with result of ZHANG et al [9]. At the same time, ZHANG et al also observed the fracture surface of rock specimens by the scanning electron microscope (SEM). The results show that the specimens with zigzag crack propagation path account for more intergranular fracture, while the specimens with straight crack propagation path account for more transgranular fracture. In this experiment, the fracture toughness of shale increases as the loading rate increases, which is mainly due to the zigzag crack propagation path of shale specimen at low loading rate; the main occurrence in the shale specimen is intergranular failure; the fracture energy required for crack propagation is less; and as the loading rate increases, the crack propagation path of shale specimen becomes straight, and the main failure mode of the shale specimen changes from intergranular failure to transgranular failure, so the fracture energy required for crack propagation also increases.

3.3 Crack propagation velocity of shale with different loading rates

Figure 8 shows the experimental results of crack propagation velocity for specimen S-3-2. It can be found from Figure 8(a) that when the prefabricated crack does not start to propagate, the voltage of CPG is kept at about 1.29 V. At 3.4 μs, the voltage of the CPG suddenly jumps to 1.59 V, indicating that the first wire of the CPG breaks. As the crack continues to propagate, the grid wire breaks in turn, and the voltage signal increases step by step. Until 67.8 μs, the CPG breaks completely, and the voltage signal no longer changes. According to the step type voltage signal, the instantaneous moment of each grid wire fracture can be determined, and then the instantaneous crack propagation velocity can be calculated according to the following equation:

$$V = \Delta L/(t_{n+1} - t_n) \tag{6}$$

where t_n is the instant moment when the n-th grid wire of CPG breaks; V is the instantaneous crack propagation velocity among t_n and t_{n+1}; ΔL is the distance between two adjacent grid wires. In this test, ΔL is 1.5 mm. The variation of the instantaneous crack propagation velocity is depicted in Figure 8(b). It can be found that the crack propagation velocity gradually decreases after a

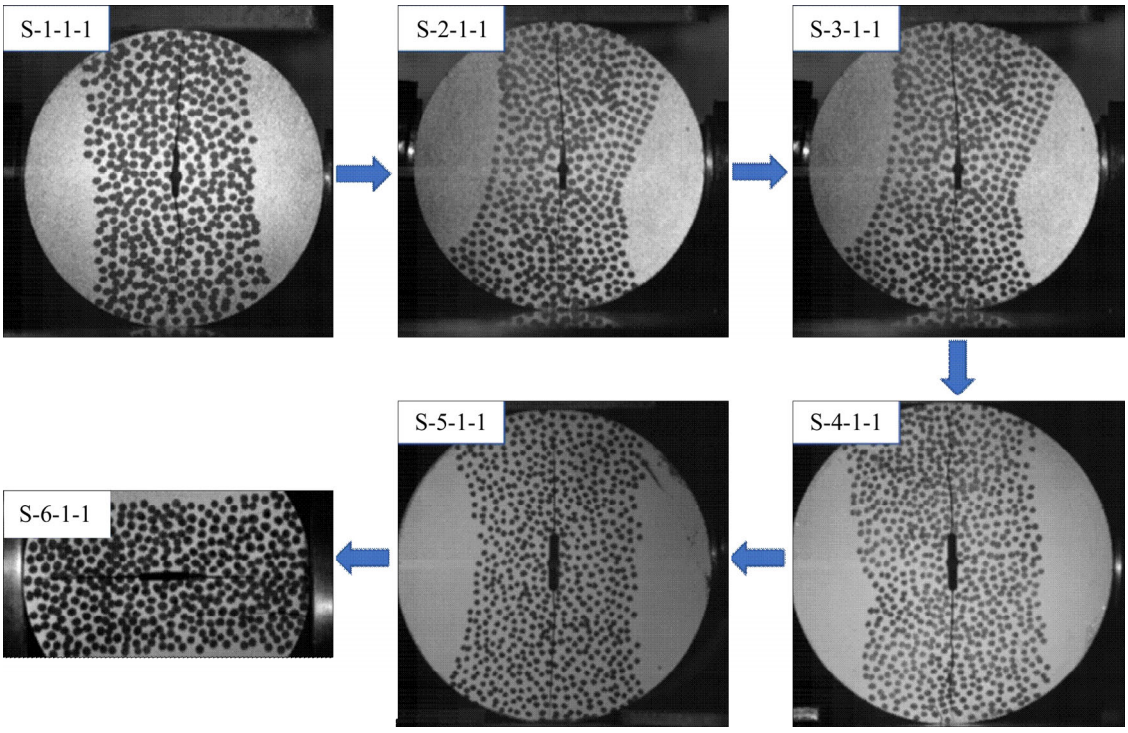

Figure 7 Failure image of shale specimens under different loading rates

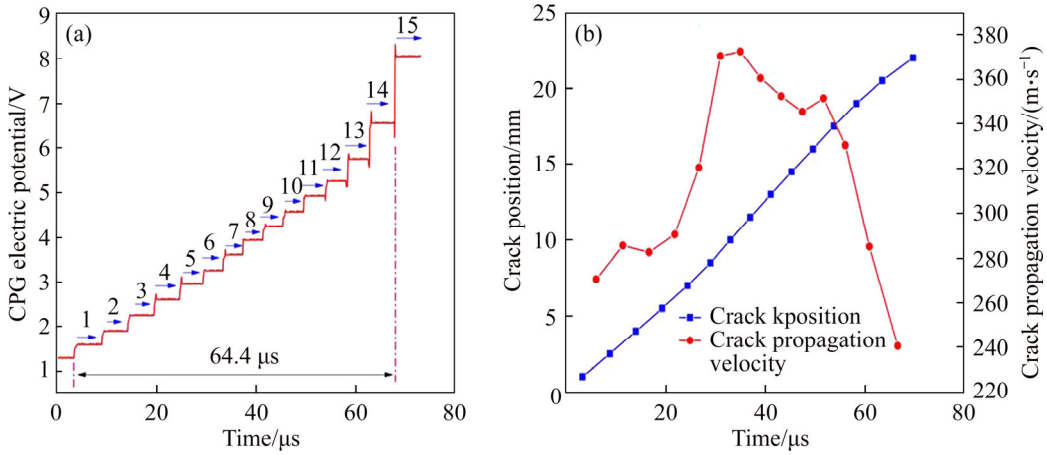

Figure 8 Test results of CPG: (a) Variation of CPG voltage signal; (b) Crack position and crack propagation velocity measured by a CPG

period of increase. The main reason is that the strain energy released at the initial stage of crack propagation is greater than the consumed surface energy. The excess energy is converted into the kinetic energy required for crack propagation, and the crack propagation velocity gradually increases. With the failure of shale specimen, the load on the specimen decreases rapidly, and the strain energy released during the crack propagation is less than the surface energy consumed. In order to maintain the crack propagation, part of the kinetic energy gradually changes to the surface energy, and the crack propagation velocity decreases. In order to facilitate the analysis, the average of these instantaneous crack propagation velocity is taken as the crack propagation velocity under a certain loading rate.

Figure 9 shows the variation of the transformed loading rate and the average crack propagation velocity of shale specimens under static loading. It can be found that there is a positive correlation between the average crack propagation velocity and the loading rate of shale specimens. After analysis and calculation, the correlation coefficient of the fitting equation of the two based on the exponential regression model reaches 0.998, which shows that the relationship between the crack propagation velocity and the transformed loading rate can be expressed as an exponential function:

$$V_{ave}=20272-20146\exp(-0.005T_{LR}) \quad (7)$$

where V_{ave} is the average crack propagation velocity at a certain loading rate. Substituting Eq. (4) into Eq. (7) yields the relationship between the original loading rate and crack propagation velocity as:

$$V_{ave}=20272-20194L_R^{-0.002} \quad (8)$$

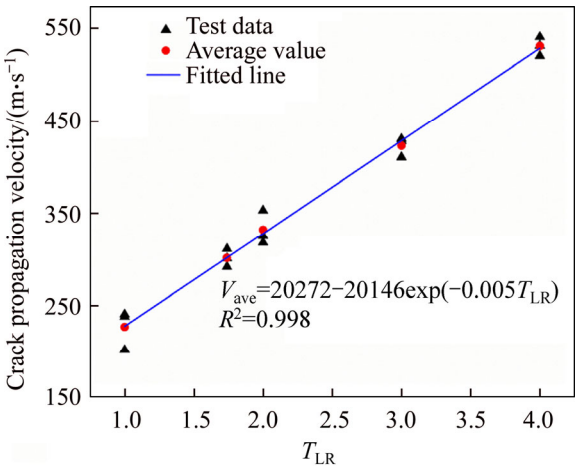

Figure 9 Variation of crack propagation velocity versus loading rates under static loading

Previous studies on crack propagation velocity have basically focused on dynamic loading conditions. In fact, the effect of loading rate on crack propagation velocity under static loading conditions is also significant. In this experiment, the average crack propagation velocity of shale specimens at a loading rate of 30 N/s is 239.2 m/s, while at a loading rate of 30000 N/s, it reaches 530.6 m/s, which is about twice the difference. According to the improved Griffith theory [40], the strain energy released by the rock during crack propagation is mainly converted into two parts, one part is used for the surface energy required for crack propagation, and the other part is converted into kinetic energy. When the rock material and size are determined, the strain energy released during crack propagation depends only on the magnitude of the external load. As the loading rate increases, the strain energy released per unit time of the rock also increases, and the surface energy is usually unchanged during the crack propagation process, so the more part of the strain energy is converted into kinetic energy, which promotes a higher crack propagation velocity at higher loading rates.

In this experiment, based on the mathematical relationship between the loading rate and the crack propagation velocity under static loading conditions, one can try to predict the crack propagation velocity under dynamic loading conditions. In the dynamic test, the predicted crack propagation velocity at a loading rate of 0.57 GN/s is 876 m/s, while the actual test crack propagation velocity is 744 m/s, and the difference between the two is 132 m/s. In fact, the crack propagation velocity will not always increase as the loading rate increases, but has a limit value. Some classic theories predict that the propagation velocity of mode I cracks will not exceed the material's Rayleigh wave speed [41, 42]. When the crack propagation velocity is large enough, more micro-cracks near the crack tip will be excited at the same time, consuming more strain energy released by the material, slowing down the tendency of crack propagation velocity to increase with increasing loading rate. In addition, when the crack propagation velocity is close to the Rayleigh wave velocity of the material, these micro-cracks

will merge to form large-scale cracks, resulting in crack bifurcation. This process dissipates most of the strain energy, which limits the increase of the crack propagation velocity.

3.4 AE characteristics

Figure 10 manifests the variation of the load, AE parameters for shale specimens with different loading rates versus time. It can be found that the AE signals at the initial stage of loading have the characteristics of low amplitude and low energy at low loading rate. With the increase of load, the internal damage of rock gradually accumulates. When it reaches the peak load, large-scale instability of rock occurs, and a large number of AE signals with high amplitude and high energy are generated. However, as the loading rate increases, the amplitude of the AE signal in the early stage of loading changes from low amplitude to high amplitude. This shows that the instability mode of rock is changing from small-scale failure to large-scale failure. In other words, under high loading rate, there is not enough time for the development of microcracks in the rock, and large-scale macrocracks are directly formed. It can be found from Figure 10 that as the loading rate

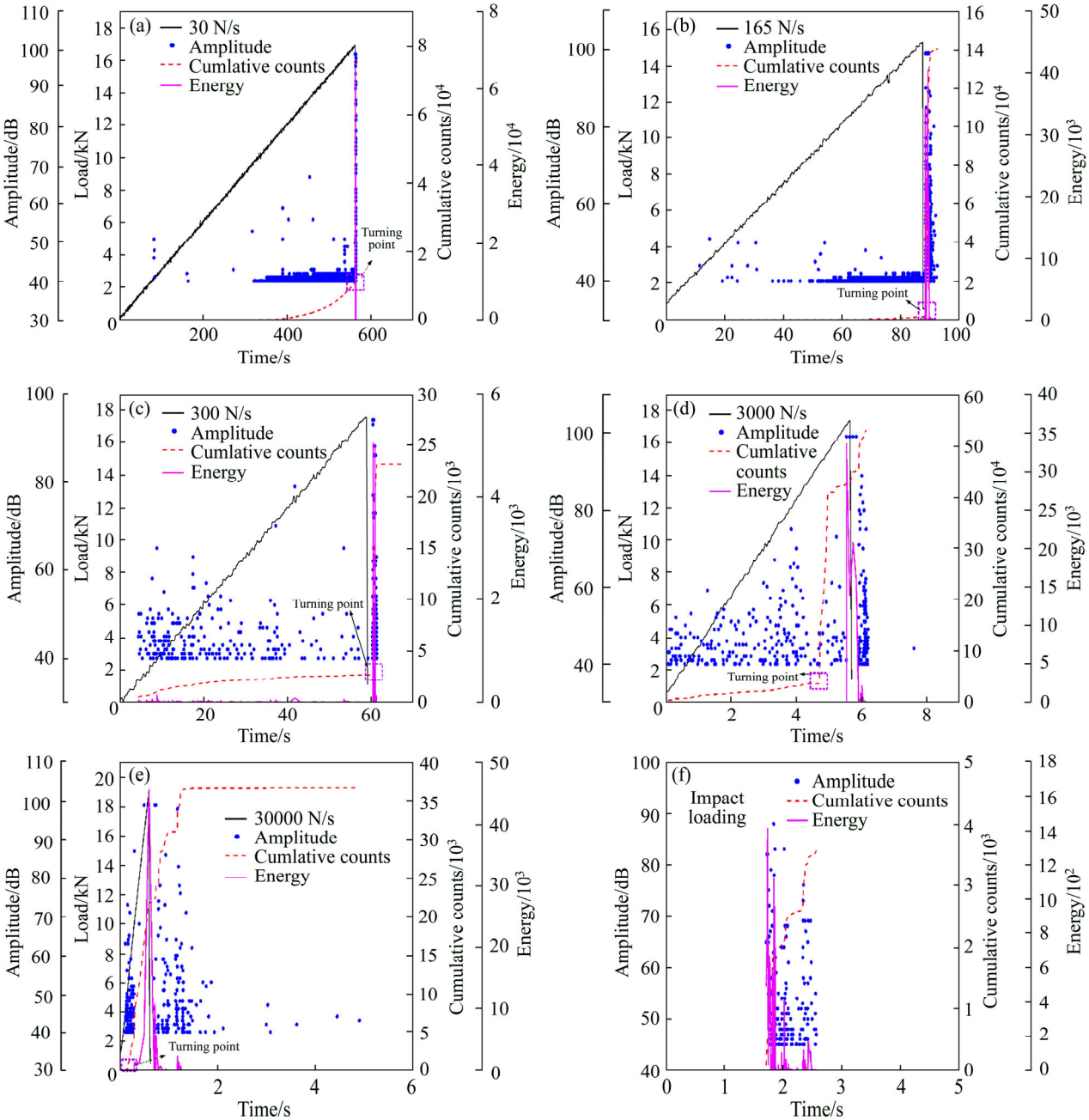

Figure 10 Curves for load, AE parameters with time at different loading rates

increases, the turning point of the cumulative AE counts moves forward. When the loading rate is 30 N/s, the turning point of the cumulative counts is near the peak load. However, when the loading rate is 30000 N/s, the turning point of the cumulative counts appears at the beginning of loading. This further indicates that at low loading rates, the recorded AE signals mainly come from the initiation and propagation of microcracks.

From the analysis of the AE signals of shale at different loading rates, it is found that at low loading rates, the AE signals generated by shale rupture mainly come from the initiation and propagation of microcracks, and with the increase of loading rates, the AE signals generated by large-scale macrocracks gradually increase. It shows that the energy used for microcracks fracture is less at high loading rate [43, 44], and the strain energy is accumulated until the moment of failure. Therefore, the energy released at the moment of specimen failure increases with the increase of the loading rate, and the fracture energy used to form new surface also increases, which leads to the enhancement of fracture toughness of shale. Meanwhile, at low loading rates, crack propagation is the process of internal microcracks initiating, propagating and gathering to form large-scale cracks. However, at high loading rates, the internal microcracks in the specimen have no time to propagate and directly form large-scale cracks. This may also be the reason that the crack propagation velocity of shale specimens at high loading rate is higher than that at low loading rate.

4 Conclusions

In this project, the fracture behavior of shale under different loading rates was studied. The effect of loading rate on crack propagation velocity and fracture toughness of shale was determined, and AE signals generated by rock fracture under different loading conditions were collected and analyzed. From this study, the following conclusions are mainly drawn:

1) From the DIC analysis results of all shale specimens, it is found that the failure processes of the specimens under different loading rates are basically similar, all of them start to crack from the tip of the prefabricated crack which will propagate towards the loading point. This also ensures the validity of the test results obtained in this experiment.

2) The fracture toughness of shale has a positive correlation with loading rate. The fracture toughness of shale increases by 25.6% when the loading rate increases from 30 N/s to 30000 N/s, which shows that the loading rate has a significant effect on the fracture toughness even under static loading conditions. In addition, the relationship between loading rate and fracture toughness can be expressed by a logarithmic function, which helps us to predict the fracture toughness of shale under different loading rates. Meanwhile, as the loading rate increases, the crack propagation path of shale specimen changes from zigzag to straight, and the fracture energy used to form a new surface increases gradually, which leads to the enhancement of fracture toughness of shale.

3) The crack propagation velocity increases with the increase of loading rate. The relationship between loading rate and crack propagation velocity under static loading can be expressed as a power function. In addition, when the crack propagation velocity exceeds a certain limit, the increasing trend of crack propagation velocity with the increase of loading rate will slow down.

4) As the loading rate increases, the AE signals generated by microcrack initiation and propagation decrease gradually, and the turning point of cumulative count moves forward. This shows that the strain energy consumed by microcracks is more at low loading rate, but as the loading rate increases, microcracks do not have enough time to develop, directly forming large-scale macro cracks, most of the strain energy is converted into the fracture energy used to form new surfaces, which also leads to the increase of shale fracture toughness. On the other hand, the increase of the loading rate causes the change of the crack propagation process inside the specimen, which may also be the reason for the change of the crack propagation velocity.

Contributors

XIE Qin is responsible for the experimental part and the paper writing. LI Sheng-xiang is responsible for the data processing and part of the

paper writing. LIU Xi-ling is responsible for experimental setup and theoretical analysis. GONG Feng-qiang and LI Xi-bing is responsible for experimental results analysis.

Conflict of interest

XIE Qin, LI Sheng-xiang, LIU Xi-ling, GONG Feng-qiang and LI Xi-bing declare that they have no conflict of interest.

References

[1] QI Cheng-zhi, WANG Ming-yang, QIAN Qi-hu. Strain-rate effects on the strength and fragmentation size of rocks [J]. International Journal of Impact Engineering, 2009, 36(12): 1355−1364. DOI: 10.1016/j.ijimpeng.2009.04.008.

[2] KUMAR A. The effect of stress rate and temperature on the strength of basalt and granite [J]. Geophysics, 1968, 33(3): 201−510. DOI: 10.1190/1.1439947.

[3] CHOCRON S, DANNEMANN K A, NICHOLLS A. Apache leap tuff rock: High strain rate characterization and support simulations [J] Journal de Physique IV (Proceedings). 2006, 134: 565−570. DOI: 10.1051/jp4:20061 34087.

[4] PATERSON M S. Experimental rock deformation-the brittle field [M]. New York, NY: Springer-Verlag, 1978: 254. DOI: 10.1007/b137431.

[5] MASUDA K, MIZUTANI H, YAMADA I. Experimental study of strain-rate dependence and pressure dependence of failure properties of granite [J]. The Seismological Society of Japan, (The Volcanological Society of Japan, The Geodetic Society of Japan), 1987, 35(1). DOI: 10.4294/jpe1952.35.37.

[6] WONG R H C, CHAU K T, TANG C A, LIN P. Analysis of crack coalescence in rock-like materials containing three flaws part I: Experimental approach [J]. International Journal of Rock Mechanics and Mining Sciences, 2001, 38(7): 909−924. DOI: 10.1016/S1365-1609(01)00064-8.

[7] GONG Feng-qiang, WU Chen. Identifying crack ompaction and crack damage stress thresholds of rock using load–unload response ratio (LURR) theory [J]. Rock Mechanics and Rock Engineering, 2020, 53(2): 943−954. DOI: 10.1007/s00603-019-01936-z.

[8] HOEK E, MARTIN C D. Fracture initiation and propagation in intact rock—A review [J]. Journal of Rock Mechanics and Geotechnical Engineering, 2014, 6(4): 287−300. DOI: 10.1016/j.jrmge.2014.06.001.

[9] ZHANG Qian-bing, ZHAO Jian. Effect of loading rate on fracture toughness and failure micromechanisms in marble [J]. Engineering Fracture Mechanics, 2013, 102(2): 288−309. DOI: 10.1016/j.engfracmech.2013.02.009.

[10] WANG Qi-zhi, FENG Feng, NI Ming-qing, GOU Xiao-ping. Measurement of mode I and mode II rock dynamic fracture toughness with cracked straight through flattened Brazilian disc impacted by split Hopkinson pressure bar [J]. Engineering Fracture Mechanics, 2011, 78(12): 2455−2469. DOI: 10.1016/j.engfracmech.2011.06.004.

[11] YIN Tu-bing, BAI Lv, LI Xiang, LI Xi-bing, ZHANG Shuai-shuai. Effect of thermal treatment on the mode I fracture toughness of granite under dynamic and static coupling load [J]. Engineering Fracture Mechanics, 2018: S0013794418302212. DOI: 10.1016/j.engfracmech.2018.05.035.

[12] ZHOU Zi-long, CAI Xin, MA Dan, DU Xue-ming, CHEN Lu, WANG Hai-quan, ZANG Hai-zhi. Water saturation effects on dynamic fracture behavior of sandstone [J]. International Journal of Rock Mechanics and Mining Sciences, 2019, 114: 46−61. DOI: 10.1016/j.ijrmms.2018.12.014.

[13] ZHOU Xiao-ping, QIAN Qi-hu, YANG Hai-qing. Effect of loading rate on fracture characteristics of rock [J]. Journal of Central South University of Technology, 2010, 17(1): 150−155. DOI: 10.1007/s11771-010-0024-4.

[14] FREUND L B. Dynamic crack propagation [C]// The Mechanics of Fracture. New York, American Society of Mechanical Engineers, 1976: 105–134. https://www.researchgate.net/publication/279767268_DYNAMIC_CRACK_PROPAGATION?ev=auth_pub.

[15] JU Ming-he, LU Jian-chun, LU Xiao-feng, ZHAO Jian. Fracture surface morphology of brittle geomaterials influenced by loading rate and grain size [J]. International Journal of Impact Engineering, 2019, 133. DOI: 10.1016/j.ijimpeng.2019.103363.

[16] FRANKLIN J A, SUN Z Q, ATKINSON B K, MEREDITH P G, RUMMEL F, MUELLER W, NISAIMATSU Y, TAKAHASHI H, COSTINL S, INGRAFFEA A R, BOBROV G F. Suggested methods for determining the fracture toughness of rock [J]. International Journal of Rock Mechanics and Mining Sciences, 1988, 25(2): 71−96. DOI: 10.1016/0148-9062(88)91871-2.

[17] FOWELL R, HUDSON J, XU C, ZHAO X. Suggested method for determining mode I fracture toughness using cracked chevron notched Brazilian disc (CCNBD) specimens [J]. International Journal of Rock Mechanics and Mining Sciences and Geomechanics Abstracts, 1995, 32(1): 57−64. DOI: 10.1016/0148-9062(94)00015-U.

[18] KURUPPU M, OBARA Y, AYATOLLAHI M, CHONG K, FUNATSU T. ISRM-suggested method for determining the mode I static fracture toughness using semi-circular bend specimen [J]. Rock Mechanics and Rock Engineering, 2014, 47. DOI: 10.1007/s00603-013-0422-7.

[19] ZHOU Ying-xin, XIA Kai, LI Xi-bing, LI Huo-bing, MA Guo-wei, ZHOU Jian, ZHOU Zi-long. Suggested methods for determining the dynamic strength parameters and mode-I fracture toughness of rock materials [J]. International Journal of Rock Mechanics and Mining Sciences, 2011, 49: 105−112. DOI: 10.1016/j.ijrmms.2011.10.004.

[20] AYATOLLAHI M R, MAHDAVI E, ALBORZI M J. Stress intensity factors of semi-circular bend specimens with straight-through and chevron notches [J]. Rock Mechanics and Rock Engineering, 2016, 49(4): 1161−1172. DOI: 10.1007/s00603-015-0830-y.

[21] YAMAUCHI Y, NAKANO M, KISHIDA K, OKABE T. Measurement of fracture toughness for brittle materials

under mixed-mode impact loading using center-notched disk specimen [J]. J Soc Mater Sci (Japan), 2000, 49(12): 1324−1329. DOI: 10.2472/jsms.49.1324.

[22] ZHOU Jun, WANG Yang, XIA Yuan-ming. Mode-I fracture toughness of PMMA at high loading rates [J]. Journal of Materials Science, 2006, 41(24): 8363−8366. DOI: 10.1007/s10853-006-0980-0.

[23] LI Xi-bing, LOK T S, ZHAO Jian. Dynamic characteristics of granite subjected to intermediate loading rate [J]. Rock Mechanics and Rock Engineering, 2005, 38(1): 21−39. DOI: 10.1007/s00603-004-0030-7.

[24] GONG Feng-qiang, ZHAO Gao-feng. Dynamic indirect tensile strength of sandstone under different loading rates [J]. Rock Mechanics and Rock Engineering, 2014, 47(6): 2271−2278. DOI: 10.1007/s00603-013-0503-7.

[25] GONG Feng-qiang, SI Xue-feng, LI Xi-bing. Dynamic triaxial compression tests on sandstone at high strain rates and low confning pressures with split Hopkinson pressure bar [J]. International Journal of Rock Mechanics and Mining Science, 2019, 113: 211−219. DOI: 10.1016/j.ijrmms.2018.12.005.

[26] PETERS W H. Digital image techniques in experimental stress analysis [J]. Optical engineering, 1982, 21(3): 427−431. DOI: 10.1117/12.7972925.

[27] ZHU Quan-qi, LI Di-yuan, HAN Zhen-yu, LI Xi-bing, ZHOU Zi-long. Mechanical properties and fracture evolution of sandstone specimens containing different inclusions under uniaxial compression [J]. International Journal of Rock mechanics and Mining Science, 2019, 115: 33−47. DOI: 10.1016/j.ijrmms.2019.01.010.

[28] ZHOU Xiao-ping, LIAN Yi-jiang, WONG L N Y, BERTO F. Understanding the fracture behavior of brittle and ductile multi-flawed rocks by uniaxial loading by digital image correlation [J]. Engineering Fracture Mechanics, 2018, 199: 438−460. DOI: 10.1016/ j.engfracmech.2018.06.007.

[29] ZHOU Xiao-ping, WANG Yun-teng, ZHANG Jian-zhi, LIU Fei-nan. Fracturing behavior study of three-flawed specimens by uniaxial compression and 3D digital image correlation: Sensitivity to brittleness [J]. Rock Mechanics and Rock Engineering, 2019, 52(3): 691−718. DOI: 10.1007/s00603-018-1600-4.

[30] ZHOU Zi-long, CAI Xin, MA Dan, CAO Wen-zhuo, CHEN Lu, ZHOU Jing. Effects of water content on fracture and mechanical behavior of sandstone with a low clay mineral content [J]. Engineering Fracture Mechanics, 2018, 193: 47−65. DOI: 10.1016/j.engfracmech.2018.02.028.

[31] ZHOU Lei, ZHU Zhe-ming, WANG Meng, YING Peng, DONG Yu-qing. Dynamic propagation behavior of cracks emanating from tunnel edges under impact loads [J]. Soil Dynamics and Earthquake Engineering, 2018, 105: 119−126. DOI: 10.1016/j.soildyn. 2017.12.012.

[32] YING Peng, ZHU Zhe-ming, WANG Fei, WANG Meng, MIU Chao-yuan, ZHOU Lei. The characteristics of dynamic fracture toughness and energy release rate of rock under impact [J]. Measurement, 2019, 147. DOI: 10.1016/j.measurement.2019.106884.

[33] GONG Feng-qiang, LUO Song, YAN Jing-yi. Energy storage and dissipation evolution process and characteristics of marble in three tension-type failure tests [J]. Rock Mechanics and Rock Engineering, 2018, 51: 3613−3624. DOI: 10.1007/s00603-018-1564-4.

[34] ZHOU Xiao-ping, ZHANG Jian-zhi, QIAN Qi-hu, NIU Yong. Experimental investigation of progressive cracking processes in granite under uniaxial loading using digital imaging and AE techniques [J]. Journal of Structural Geology, 2019, 126: 129−145. DOI: 10.1016/j.jsg.2019.06.003.

[35] ZHOU Xiao-ping, ZHANG Jian-zhi, BERTO F. Fracture analysis in brittle sandstone by digital imaging and AE techniques: Role of flaw length ratio [J]. Journal of Materials in Civil Engineering, 2020, 32(5): 04020085. DOI: 10.1061/(ASCE)MT.1943-5533.0003151.

[36] ZHANG Jian-zhi, ZHOU Xiao-ping. AE event rate characteristics of flawed granite: From damage stress to ultimate failure [J]. Geophysical Journal International, 2020, 222(2): 795−814. DOI: 10.1093/gji/ggaa207.

[37] MANTHEI G, EISENBLÄTTER J. Acoustic emission in study of rock stability [M]. Berlin Germany: Springer Berlin Heidelberg, 2008: 236−310. DOI: 10.1007/978-3-540-69972-9_11.

[38] WU Chen, GONG Feng-qiang, LUO Yong. A new quantitative method to identify the crack damage stress of rock using AE detection parameters [J]. Bulletin of Engineering Geology and the Environment, 2020, 5. DOI:10.1007/s10064-020-01932-6.

[39] China Aviation Academy. Handbook of stress intensity factors [M]. Beijing: Science Press, 1981: 174−179. (in Chinese)

[40] GRIFFITH A A. The phenomena of rupture and flow in solids [J]. Philosophical Transactions of The Royal Society. A Mathematical Physical and Engineering Sciences, 1921, 221: 163−198. DOI: 10.1098/rsta.1921.0006.

[41] FREUND L B. Dynamic fracture mechanics [M]. The Edinburgh Building, United Kingdom: Cambridge University Press, 1998: 367−437. https://scholar.chongbuluo.com/.

[42] BROBERG K B. Crack and fracture [M]. Ireland: Academic Press, 1990: 509−543. https://www.sciencedirect.com/book/9780121341305/cracks-and-fracture.

[43] LIU Xi-ling, LI Xi-bing, HONG Liang, YIN Tu-bing, RAO Meng. Acoustic emission characteristics of rock under impact loading [J]. Journal of Central South University, 2015, 22: 3571−3577. DOI: 10.1007/s11771-015-2897-8.

[44] LIU Xi-ling, LIU Zhou, LI Xi-bing, GONG Feng-qiang, Du Kun. Experimental study on the effect of strain rate on rock acoustic emission characteristics [J]. International Journal of Rock Mechanics and Mining Sciences, 2020, 133: 104420. DOI: 10.1016/j.ijrmms.2020.104420.

(Edited by HE Yun-bin)

中文导读

加载速率对 I 型加载下页岩断裂行为的影响

摘要：本研究从动态和静态加载条件下考察了加载速率对页岩断裂行为的影响。在纯 I 型加载条件下采用分离式的 SHPB 杆和 INSTRON1346 伺服试验机对页岩试样进行了测试。在测试过程中，使用高速摄影仪和声发射采集系统分别对试样破坏过程和试样破坏产生的声发射信号进行监测，同时，通过裂纹扩展仪(CPG)测量裂纹扩展速度。结果表明，页岩的断裂韧度和裂纹扩展速度与加载速率呈正相关。在静态载荷条件下建立了断裂韧度和裂纹扩展速度与加载速率之间的关系。另外，还对不同加载速率下的声发射信号特征进行了分析。发现随着加载速率的增加，微裂纹扩展产生的声发射信号减小，同时，声发射累积计数的突变点随着加载速率的增加而向前移动，这表明低加载速率下页岩破裂产生的声发射信号主要来自微裂纹的萌生和扩展，而高加载速率下则主要来自宏观大尺度裂纹的形成。根据声发射信号的分析结果，探讨了引起页岩断裂韧度和裂纹扩展速度随加载速率变化的断裂机理。

关键词：页岩；加载速率；CSTBD；断裂韧度；声发射；裂纹扩展速度